Thermoelectric properties of Al-doped ZnO as a promising oxide material for high-temperature thermoelectric conversion

Toshiki Tsubota, Michitaka Ohtaki, Koichi Eguchi and Hiromichi Arai*

Department of Materials Science and Technology, Graduate School of Engineering Science, Kyushu University, 6-1 Kasugakoen, Kasuga, Fukuoka 816, Japan

The thermoelectric properties of a mixed oxide $(Zn_{1-x}Al_x)O$ ($x=0$, 0.005, 0.01, 0.02, 0.05) are investigated in terms of materials for high-temperature thermoelectric conversion. The electrical conductivity, σ, of the oxide increases on Al-doping by more than three orders of magnitude up to *ca.* 10^3 S cm^{-1} at room temperature, showing metallic behaviour. The Seebeck coefficient, S, of $(Zn_{1-x}Al_x)O$ ($x>0$) shows a general trend in which the absolute value increases gradually from *ca.* -100 μV K^{-1} at room temperature to *ca.* -200 μV K^{-1} at 1000 °C. As a consequence, the power factor, $S^2\sigma$, reaches *ca.* 15×10^{-4} W m^{-1} K^{-2}, the largest value of all reported oxide materials. The thermal conductivity, κ, of the oxide decreases with increasing temperature, owing to a decrease in the lattice thermal conductivity which is revealed to be dominant in the overall κ. In spite of the considerably large values of κ, the figure of merit, $Z=S^2\sigma/\kappa$, reaches 0.24×10^{-3} K^{-1} for $(Zn_{0.98}Al_{0.02})O$ at 1000 °C. The extremely large power factor of $(Zn_{1-x}Al_x)O$ compared to other metal oxides can be attributed to the high carrier mobility revealed by the Hall measurements, presumably resulting from a relatively covalent character of the Zn—O bond owing to a fairly small difference of the electronegativities of Zn and O. The dimensionless figure of merit, ZT, of 0.30 attained by $(Zn_{0.98}Al_{0.02})O$ at 1000 °C demonstrates the potential usefulness of the oxide.

Thermoelectric power generation converts thermal energy directly to electrical energy *via* the Seebeck effect induced by a temperature difference in solid materials. The energy balance of thermoelectric conversion gives the figure of merit, $Z=S^2\sigma/\kappa$, where σ is the electrical conductivity, S is the Seebeck coefficient and κ is the thermal conductivity of the material. Practical applications generally require $Z\geqslant1\times10^{-3}$ K^{-1}. On the other hand, the Carnot efficiency of thermoelectric conversion improves with an increasing temperature difference over which the thermoelectric device operates. A product of Z and the absolute temperature, the dimensionless figure of merit, ZT, is thereby employed as the most inclusive criterion for evaluating thermoelectric materials. Efficient materials have ZT values of nearly unity or greater. $ZT=1$ corresponds to a conversion efficiency $>10\%$; no materials have achieved $ZT=2$ to date.

In the last three decades, Si–Ge alloys,[1] several metal chalcogenides,[2,3] transition-metal disilicides[4–6] and some boron compounds[7,8] have been developed as materials for high-temperature thermoelectric power generation. However, practical utilization has been limited because many of these materials require costly surface protection to prevent oxidation or vaporization, and some others have inherent temperature limits owing to phase transitions at high temperatures. With respect to high-temperature operation in air, the advantages of metal oxides in their common oxidation state are apparent because of their excellent stability to heat. Moreover, a number of metal oxides have high electrical conductivities, and also the Seebeck effect in oxide materials has been studied widely. Nonetheless, reports on the application of oxides to thermoelectric materials are surprisingly scarce. While high-temperature superconducting cuprates were once proposed for thermoelectric refrigerators,[9] they were revealed to have inherently poor performances[10,11] mainly due to their extremely low carrier mobilities (as low as 0.1 cm^2 V^{-1} s^{-1}). Metal oxides are generally considered to be low-mobility materials, mainly because of their highly ionic characters. In fact, however, some oxides show considerably high carrier mobilities, *e.g.* a reported value of the Hall mobility of SnO_2 single crystals is 150–240 cm^2 V^{-1} s^{-1} at 300 K,[12] which is much larger than the value of 30 cm^2 V^{-1} s^{-1} (which is the same as the drift mobility of copper) reported for ReO_3,[13] which shows completely metallic behaviour and the highest electrical conductivity of all the known oxides in the normal state. With respect to these advantages of oxide materials, we have begun to investigate the thermoelectric properties of oxides, and have reported already that In_2O_3-based mixed oxides[14] and $CaMnO_3$-based perovskite-type oxides[15] have potential for new thermoelectric materials at high temperatures.

Zinc oxide is well known as a conductive oxide with a wide forbidden bandgap of 3.5 eV. The electrical properties of ZnO have attracted much interest in many fields related to chemistry and physics, and are applied to electronic devices such as gas sensors[16] and varistors.[17] Although Zn is sometimes regarded as a member of the 3d transition metals, ZnO is actually not a transition metal oxide because the 3d orbital of Zn^{2+} is filled. In general, the valence band of a metal oxide semiconductor consists mainly of the 2p orbital of the O^{2-} anions, while an empty or half-filled orbital with the lowest energy in the metal cations dominates the characteristics of the conduction band. The conduction electrons in the 3d transition-metal oxides are therefore largely influenced by a localized character of the 3d orbitals of the metal cations. However, the conduction band of ZnO is constituted mainly of the lowest unoccupied 4s and 4p orbitals of Zn^{2+}, and thus the conduction electrons would be more mobile. The fairly large electronegativity of Zn, and its relatively small ionicity as well as a strong preference for the sp^3 hybridization of the Zn—O bond also appear to be very promising, since they imply that the Zn—O bond has a rather covalent character, which would lead to a high carrier mobility in the oxide. In the present study, we have investigated the thermoelectric properties of ZnO-based mixed oxides in terms of thermoelectric power generation at high temperatures, revealing the highly promising thermoelectric figure of merit of Al-doped ZnO for the first time as an oxide material.[18] Here we discuss the thermoelectric properties in terms of the electrical and thermal transport properties, analytical and spectroscopic information, and we consider the microstructures of the oxide as a potential material for high-temperature thermoelectrics.

Experimental

Preparation and characterization of samples

The mixed oxides $(Zn_{1-x}Al_x)O$ ($x=0$, 0.005, 0.01, 0.02, 0.05) were prepared from ZnO and Al_2O_3 powders of guaranteed grade. The powders were mixed and pulverized in a Nylon-lined ball mill for 24 h. The powder mixture was pressed into a pellet and sintered at 1400 °C for 10 h in air. The heating and cooling rates were 200 °C h^{-1}. The crystal phases in the samples thus obtained were examined by a powder X-ray diffraction (XRD) study on a Rigaku RINT-1400 diffractometer using Cu-Kα radiation. Scanning electron microscopy was carried out on a JEOL JSM-T330A instrument equipped with an EDX spectrometer. Auger microprobe analysis was performed on a field emission type JEOL JAMP-7800F spectrometer operated at a probe energy of 10 keV. ^{27}Al solid-state NMR spectra were collected on a Varian VXR-400S spectrometer at an oscillation frequency of 104.21 MHz using the MAS technique at room temperature. An $AlCl_3$ aqueous solution was employed as an external reference (δ −0.1). A single pulse sequence with a delay time (D_1) of 2.0 s was applied.

Measurement of thermoelectric properties

The samples for electrical measurements were cut from the sintered pellets as rectangular bars of *ca.* $15\times5\times3$ mm^3, and polished with SiC emery papers. The relative densities of all the samples were measured by Archimedes' method. The measurements of the electrical conductivity and the Seebeck coefficient were carried out simultaneously in air from room temperature to 1000 °C. The measurement procedures have been described elsewhere in detail.[14] Briefly, the σ values were measured by the dc four-probe technique. The S values were obtained from the least-squares regressions of the thermoelectromotive force as a function of the temperature difference <5 K applied by a heater at each measurement temperature. All the measurements were carried out after attaining the steady-state temperature at each step. The carrier concentration, n, and the Hall mobility, μ_H, were determined from the Hall measurements carried out at room temperature by the van der Pauw method for sliced samples at an applied magnetic field of 0.8 T. The thermal conductivity was determined from the thermal diffusivity and the specific heat capacity obtained by the laser flash measurement on an ULVAC TC-7000 instrument from room temperature to 1000 °C for sample disks 10 mm in diameter and 1–2 mm in thickness. The κ data were calibrated with a standard sample of a sapphire single crystal.

Results and Discussion

Electrical transport properties

The temperature dependence of the electrical conductivity, σ, of $(Zn_{1-x}Al_x)O$ ($x=0$, 0.005, 0.01, 0.02, 0.05) is shown in Fig. 1. The σ value of undoped ZnO increased sharply with increasing temperature to 700 °C, and appeared rather constant between 700 and 1000 °C. The Arrhenius plot of σ for undoped ZnO indicates that the sample has an impurity region up to 700 °C, showing no intrinsic conduction up to 1000 °C. With the addition of a small amount of Al_2O_3 ($x=0.005$), the behaviour of σ changed from semiconducting to metallic, and the values became higher than that for undoped ZnO by more than three orders of magnitude at room temperature. The σ values of $(Zn_{1-x}Al_x)O$ showed a monotonic increase with increasing amounts of added Al_2O_3 up to $x=0.02$, and then decreased slightly on further Al-doping, as seen for $x=0.05$. Consequently, $(Zn_{0.98}Al_{0.02})O$ gave the highest σ value of all the samples. Because all the sintered samples, including the undoped one, have a dense microstructure with a relative density >99%, density difference between the samples cannot explain the variation in σ. The incorporation of Al into ZnO should therefore be responsible for the noticeable changes of the value and the behaviour of σ observed here.

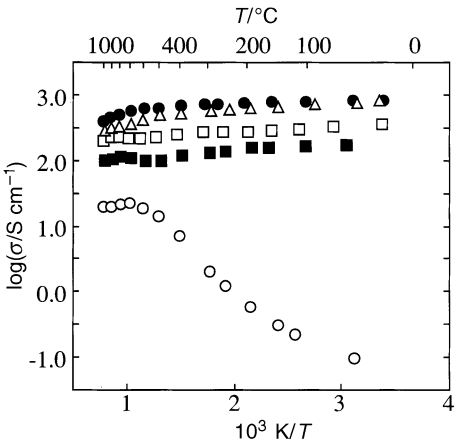

Fig. 1 Arrhenius plots for the electrical conductivities of $(Zn_{1-x}Al_x)O$ for $x=0$ (○), 0.005 (■), 0.01 (□), 0.02 (●), 0.05 (△)

The Seebeck coefficients, S, of $(Zn_{1-x}Al_x)O$ ($x=0$, 0.005, 0.01, 0.02, 0.05) are shown in Fig. 2. The S values of all the samples are negative within the whole temperature range examined, indicating n-type conduction. The Seebeck coefficient of undoped ZnO has large and negative values of *ca.* −300 to −400 μV K^{-1} from room temperature to 1000 °C, and showed no particular dependence on temperature. On the other hand, $(Zn_{1-x}Al_x)O$ ($x>0$) gave smaller but still moderate S values, with a general trend in which the absolute value increased gradually from *ca.* −100 μV K^{-1} at room temperature to *ca.* −200 μV K^{-1} at 1000 °C.

The power factor, $S^2\sigma$, which represents the electrical contribution to the overall thermoelectric performance, is calculated from the results obtained above and depicted in Fig. 3 as a function of temperature. The $S^2\sigma$ value of undoped ZnO increases with increasing temperature owing to a large increase in σ. The maximum $S^2\sigma$ value of undoped ZnO is 3.68×10^{-4} W m^{-1} K^{-2} at 1000 °C; even this value appears to be surprisingly large compared with those shown by oxide materials. All the Al-doped samples, nonetheless, attain exceedingly large values of $S^2\sigma$, *i.e.* $8–15\times10^{-4}$ W m^{-1} K^{-2} over a wide temperature range from room temperature to 1000 °C. These values are the largest ever reported on oxide materials, and also surpass those shown by β-$FeSi_2$ and β-SiC,[19] which have been proposed as non-oxide candidates for high-temperature thermoelectric materials. The unexpectedly large power factor of $(Zn_{1-x}Al_x)O$ denotes the superiority of the electrical

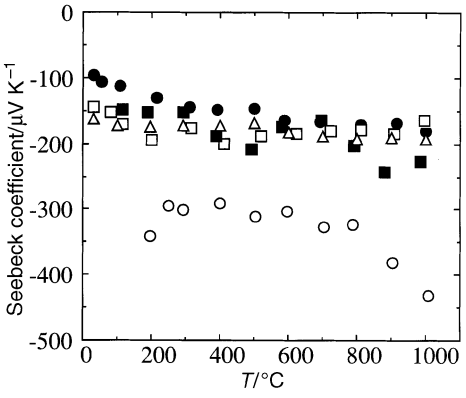

Fig. 2 The Seebeck coefficients of $(Zn_{1-x}Al_x)O$ as a function of temperature for $x=0$ (○), 0.005 (■), 0.01 (□), 0.02 (●), 0.05 (△)

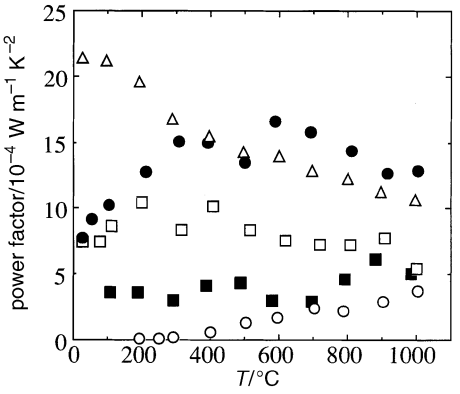

Fig. 3 The power factors of $(Zn_{1-x}Al_x)O$ as a function of temperature for $x=0$ (○), 0.005 (■), 0.01 (□), 0.02 (●), 0.05 (△)

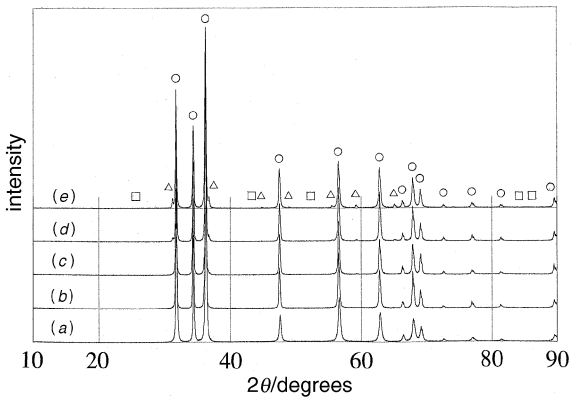

Fig. 4 Powder X-ray diffraction patterns of $(Zn_{1-x}Al_x)O$ for $x=0$ (*a*), 0.005 (*b*), 0.01 (*c*), 0.02 (*d*), 0.05 (*e*). ○, ZnO; △, $ZnAl_2O_4$; □, α-Al_2O_3.

transport properties of the present oxide in contrast to a general view of metal oxides as ionic solids.

We also carried out Hall measurements to investigate the carrier concentration and the mobility of each sample. The carrier concentrations, n, of $(Zn_{1-x}Al_x)O$ ($x=0$, 0.005, 0.01, 0.02, 0.05) at room temperature are shown in Table 1. Assuming that all Al atoms occupy Zn sites in ZnO and that they act as donors to provide one electron per Al, theoretical values of n can also be calculated from the amount of doped Al_2O_3. Whereas the observed n value for undoped ZnO is of the order of 10^{23} m^{-3}, all of the observed n values for the Al-doped samples are of the order of 10^{25} m^{-3}. The dramatic increase in the observed n values brought about by Al-doping is consistent with the marked increase in σ accompanying the semiconductor-to-metal transition seen in Fig. 1. However, the observed n value appears to be almost saturated at $x\approx0.005$, being smaller than the theoretical values even at $x=0.005$. These results suggest that, at higher doping levels, only a limited portion of the added Al might be effective as a dopant.

Phase, structural and spectroscopic considerations

Phase diagrams reported previously on the ZnO–Al_2O_3 system tell us that there is no solid solution region near the ZnO end member. A recent article on the phases in the system Al_2O_3–ZnO also concluded that Al_2O_3 does not dissolve in ZnO.[20] However, as mentioned above the addition of Al_2O_3 to ZnO has been regarded as a typical example of n-type doping or valence control of semiconductors.[21] Studies on phase diagrams are generally carried out with compositional changes at intervals of at least a few mol%, which appear to be too large to examine the occurrence of solid solutions at very low doping levels. The results of an XRD study for $(Zn_{1-x}Al_x)O$ ($x=0$, 0.005, 0.01, 0.02, 0.05) are shown in Fig. 4. The diffraction patterns indicate that the samples at $x\geqslant0.02$ contain a small amount of a $ZnAl_2O_4$ spinel phase which increases with increasing x. No Al_2O_3 single phase was detected for all the compositions examined. A single-phase sample of $ZnAl_2O_4$ was also prepared, and the spinel was revealed to have a high electrical resistivity. We therefore concluded that, even with a fraction smaller than the nominal compositions, a solid solution of Al_2O_3 in ZnO occurs. The $ZnAl_2O_4$ phase with high resistivity would be, however, responsible for the decrease in σ at $x=0.05$.

Table 1 The carrier concentrations of $(Zn_{1-x}Al_x)O$ at room temperature

	$n/10^{25}$ m^{-3}	
x	observed	theoretical
0	0.052	—
0.005	6.5	18
0.01	7.7	37
0.02	7.2	74
0.05	6.5	193

We have also carried out EDX and Auger microprobe analyses for cross-sections of the samples, and detected no signals due to elements other than Zn, Al and O (except surface carbon contamination). This ruled out any unintentional doping of impurities other than Al as a reason for the increase in σ. Although the low doping levels caused some difficulties in the determination of the precise concentrations of Al in the samples, the intensity ratios of Zn/Al in the EDX spectra were in good agreement with the nominal compositions, within experimental error. Two-dimensional Auger microprobe mapping for the cross-sectioned surface of $(Zn_{0.98}Al_{0.02})O$ over an area of 70×70 μm^2 with a 256×256 resolution (corresponding to a spatial resolution <300 nm) showed random distributions of Zn and Al with no correlation, confirming a sufficient homogeneity of the sample composition. Auger microprobe spectroscopy (probe diameter 15 nm) detected no difference between the elemental compositions within the grains and at the grain boundaries of the sample, thus presenting no evidence of secondary phase segregation at the grain boundary.

Furthermore, we performed ^{27}Al solid-state NMR spectroscopy in order to clarify the site and chemical environment at which the doped Al atoms might be located. Because the Zn atoms in ZnO are four-coordinated, it is expected that the coordination number of the doped Al would be four if they substitute successfully the Zn sites in ZnO. By contrast, in α-Al_2O_3, which is the thermodynamically stable phase of aluminium oxide at temperatures >1000 °C, the Al atoms are all six-coordinated, Al(6). It is well known that Al(4) and Al(6) can be distinguished easily by ^{27}Al NMR spectroscopy, because in oxides the chemical shift of the former is in the range δ 50–77, while the latter appears at δ 0–20.[22] Although the Al atoms in the $ZnAl_2O_4$ spinel are also six-coordinated, the crystallographic symmetry around the atoms should be different from those in α-Al_2O_3. Accordingly, as shown in Fig. 5(*d*) and (*e*), ^{27}Al MAS NMR spectra of α-Al_2O_3 gave a completely symmetric single peak at δ 12.5, while $ZnAl_2O_4$ showed a single peak split into an asymmetric doublet at δ 7 and 14, ascribed to second-order nuclear quadropole interaction, which can be observed well for nuclei with the nuclear spin $|I|>1$ and a large nuclear quadropole coupling constant.[23] Both spectra contain no signals due to Al(4). The Al-doped samples of $(Zn_{1-x}Al_x)O$ at $x\geqslant0.02$ showed two distinct features in their NMR spectra, as seen in Fig. 5(*b*) and (*c*); a doublet at δ 7 and 14, the same as for $ZnAl_2O_4$, and a broad resonance in the region δ 30–50 which is assigned to Al(4). However, no peak was observed in the lower field region of $\delta\geqslant60$, where Al(4) of γ-Al_2O_3 is reported to appear at δ 68.1 and is actually found at δ 67 in our experiment. These results indicate clearly

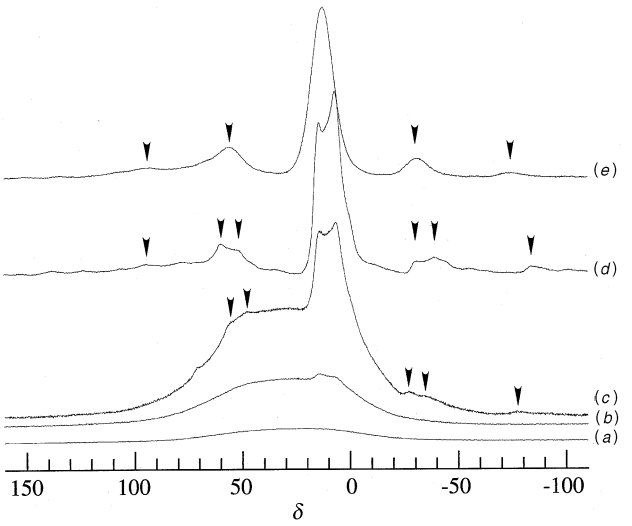

Fig. 5 ^{27}Al MAS NMR spectra of (*a*) $x=0.005$, (*b*) $x=0.02$, (*c*) $x=0.10$ for $(Zn_{1-x}Al_x)O$ and (*d*) $ZnAl_2O_4$, (*e*) α-Al_2O_3. Arrowheads indicate the spinning side bands.

the formation of the spinel phase at least at $x \geqslant 0.02$ and the absence of any Al_2O_3 single phase in all the samples, which is consistent with the XRD results. The Al(4)/Al(6) intensity ratio became larger for smaller amounts of added Al_2O_3. At very low doping levels, a weak but very broad 'bump' due to the sample probe of the NMR spectrometer overlaps in the region δ 10–50, as observed for $x=0.005$ in Fig. 5(*a*); the sample at $x=0.01$ also gave virtually the same spectrum as Fig. 5(*a*). However, differential spectra, obtained by subtracting the background spectrum measured for a ZnO raw powder, revealed that Al(4) with a peak at δ *ca.* 48 is dominant at $x=0.005$. These findings confirm that, at least at the lower doping levels, a substantial proportion of the doped Al really exists as Al(4) which should be absent in $ZnAl_2O_4$ and α-Al_2O_3, and that they have settled in an environment which is different from those for Al(4) in γ-Al_2O_3; this suggests strongly that the Al atoms occupy the Zn sites in ZnO. Even at this composition, however, there seems to be a small peak at δ *ca.* 14, implying that the spinel phase coexists even at the lowest doping level in this study. These results are in good agreement with the results of the *n* measurements stated above, in which the *n* values were practically unchanged on addition of increasing amounts of Al_2O_3 ($x>0.005$), also suggesting that the solubility limit of Al into ZnO is actually $x<0.005$. However, σ of the Al-doped ZnO increased until $x=0.02$. This fact seems to require an additional explanation.

The Hall mobility, μ_H, of $(Zn_{1-x}Al_x)O$ at room temperature was determined by Hall measurements and the results are shown in Fig. 6 as a function of *x*. The μ_H value of undoped ZnO, 65 $cm^2\ V^{-1}\ s^{-1}$, is quite reasonable compared to the values in the literature,[21] and appears to be rather large for an oxide ceramic. However, the μ_H values for the samples at $x=0.005$ and 0.01 are about half of that for undoped ZnO, and the further addition of Al caused the μ_H values to recover. These phenomena may be associated with changes in the sample microstructures. We therefore examined the microstructures of $(Zn_{1-x}Al_x)O$ ($x=0$, 0.005, 0.01, 0.02, 0.05) by SEM. The samples, polished to obtain mirror-like surfaces, were heated at 1200 °C for 20 min in air for heat etching. Undoped ZnO has a simple microstructure with large grains without noticeable interior structures. However, at $x=0.005$ the grains showed a fine-layered interior structure, and at $x=0.01$ the cross-sectional surface became roughened with a small pointed particle-like structure. We consider that these structures are responsible for the decrease in μ_H because they can provide many more scattering centres than undoped ZnO. On further

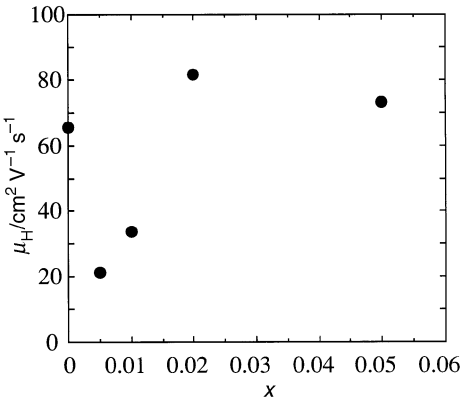

Fig. 6 The Hall mobility of $(Zn_{1-x}Al_x)O$ at room temperature as a function of *x*

addition of Al, the samples at $x=0.02$ and 0.05 showed similar microstructures in which the grain sizes are comparable to that of undoped ZnO and the grain interior appeared to be rather even. The variation in μ_H may be due to the changes in the microstructure observed here, although the reasons for these phenomena are still unclear. The changes in σ as a whole may be explained as follows: at a low doping level, incorporation of Al atoms into the Zn sites dramatically increased the carrier concentration but suppressed the mobility by changing the microstructure, and then further Al-doping caused an improvement in the microstructure, resulting in recovery of the mobility and an additional increase in σ until the secondary spinel phase came to affect the conductivity. These results also imply that the electrical properties of the oxide might be improved further by optimizing the microstructure.

Thermal transport properties

The thermal conductivity, κ, is another fundamental parameter for the evaluation of the thermoelectric performance of materials, and it may cancel out an advantage brought about by a large value of σ as is in the case for metals. Actually, the κ values of the present oxides are rather high, *ca.* 40 W m^{-1} K^{-1} at room temperature, whereas they decrease to *ca.* 5 W m^{-1} K^{-1} at 1000 °C with increasing temperature as shown in Fig. 7. In general, the thermal conductivity of metal oxides becomes higher as the atomic mass ratio M/O (M is a metal atom) approaches unity. Also, a smaller unit cell or a simpler lattice structure results in improved thermal conduction due to lattice vibrations or phonons. The lattice structure of ZnO, which forms the wurtzite structure with simple hexagonal symmetry, would hence largely be responsible for the high thermal conductivity values. Since thermoelectric materials in practical use generally have κ values of *ca.* 1–3 W m^{-1} K^{-1},

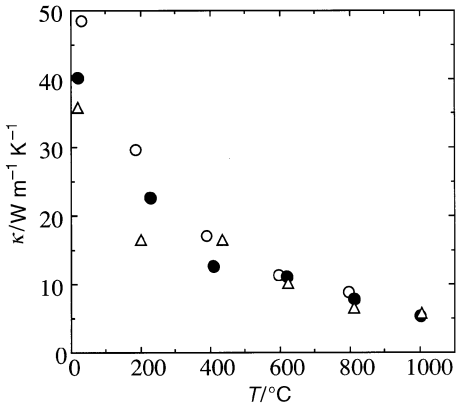

Fig. 7 The thermal conductivities of $(Zn_{1-x}Al_x)O$ as a function of temperature for $x=0$ (○), 0.02 (●), 0.05 (△)

the present κ values for $(Zn_{1-x}Al_x)O$ appear to be too high for thermoelectric applications.

Thermoelectric performance

In spite of the high κ values, the figure of merit, $Z=S^2\sigma/\kappa$, of the present oxide is revealed to be still prospective, benefiting from the considerably large power factors. The figures of merit of $(Zn_{1-x}Al_x)O$ ($x=0$, 0.02, 0.05) are shown in Fig. 8 as a function of temperature. The Z values of $x=0.02$ and 0.05 increased with increasing temperature, and Z attained the largest value of 0.24×10^{-3} K^{-1} at 1000 °C for $x=0.02$. This value is much larger than that of β-SiC,[19] and is as large as that of the best result reported on β-$FeSi_2$[4–6] which shows a maximum at *ca.* 600 °C. These facts suggest strongly that the electrical properties of the present oxide would be sufficiently advantageous to overcome the unfavourable thermal properties.

The three parameters defining the figure of merit, σ, S and κ, are all functions of the carrier concentration. Assuming that the broad-band semiconductor model holds good, an increase in the carrier concentration makes σ increase while $|S|$ decreases. According to Ioffe,[24] at a constant carrier concentration the Z value is determined by a material factor, β, defined as

$$\beta = T^{5/2}\, m^{*3/2}\, \mu/\kappa_{ph}$$

where T is the absolute temperature, m^* is the effective mass of the carrier, μ is the mobility, and κ_{ph} is the lattice thermal conductivity. This equation indicates that a large effective mass and a high mobility, as well as a small lattice thermal conductivity, are desirable. Although higher carrier mobility generally requires a smaller effective mass, an increase in the mobility overcomes the corresponding decrease in the effective mass when the dominant carrier scattering mechanism is impurity scattering rather than acoustic phonon scattering.[25] The small difference of the electronegativity between the constituent atoms generally increases the mobility. Moreover, heavy atoms and a large unit cell reduce the lattice thermal conductivity. Caillat *et al.* investigated the binary compounds on the basis of these concepts, and discovered skutterudite-related compounds having extremely high mobilities, $CoSb_3$,[26] $IrSb_3$[27] and $RuSb_2$[28] *etc.*, as potential materials for the next generation of thermoelectrics.

As mentioned above, ZnO consists of rather light atoms and has a simple crystal structure and, accordingly, the ZnO-based oxide showed a high thermal conductivity. However, the fairly small electronegativity difference between Zn and O should lead to a more covalent character of the M—O bond compared to those in other metal oxides. The ratio of the ionic radii, r(cation)/r(anion), for Zn^{2+} and O^{2-} is 0.53. Since six-coordinate geometry requires a ratio >0.414, one can expect six-coordinate Zn^{2+} in ZnO if the Zn—O bond is sufficiently ionic. However, in reality ZnO crystallizes in the wurtzite structure in which Zn^{2+} coordinates with four oxygen atoms. The sp^3 hybrid character of Zn^{2+}, in which the cations have the d^{10} closed shell and show the strongest four-coordination preference of the first-row transition metals, results in the strong directionality of the M—O bond required for the wurtzite structure. Accordingly, Zn forms a chemical bond with a rather covalent character even in its oxide; the ionicity, which is the proportion of an ionic character in an M—O bond, is reported to be 0.62 for ZnO in contrast to 0.84 for MgO in the rocksalt structure.[29] The unexpectedly large Z value of $(Zn_{1-x}Al_x)O$ should be attributed to these facts, which would lead to a high carrier mobility.

The thermal conductivity can be varied greatly by extrinsic factors such as microstructures and impurities. The overall κ value of a solid is given as

$$\kappa = \kappa_{el} + \kappa_{ph}$$

where κ_{el} and κ_{ph} are the electron and lattice thermal conductivities, respectively. It is well known that κ_{ph} is proportional to T^{-1} above the Debye temperature (this is usually below room temperature).[30] The temperature dependence of κ of $(Zn_{0.98}Al_{0.02})O$ shows a good linearity *vs.* T^{-1}, as shown in Fig. 9, suggesting a predominant contribution of κ_{ph} to the overall κ. This is further confirmed in Fig. 9 by a negligible proportion of κ_{el} estimated from the Wiedemann–Franz relation, $\kappa_{el}=L\sigma T$ (L is the Lorentz number), for which the validity for several electronic-conducting oxides has also been confirmed.[31] It is also known that for semiconductors the electronic contribution in κ is a few percent at most, and the lattice contribution is at least 90% of the overall thermal conductivity, in good agreement with the results obtained here. A suppression of κ_{ph} is therefore desirable for efficient reduction of the thermal conductivity of $(Zn_{1-x}Al_x)O$ without seriously affecting the electrical properties. This strategy is supported by our experimental results for κ in Fig. 7, in which the κ value decreases with increasing amounts of added Al_2O_3, even with the considerable increase in σ.

The temperature dependence of the dimensionless figure of merit, ZT, is shown in Fig. 10. The ZT values for $x=0.02$ and 0.05 are much larger than that of undoped ZnO over the whole temperature range. The sample at $x=0.02$ attains the largest ZT value of 0.30 at 1000 °C, in spite of its high thermal conductivity. The thermoelectric performance of the oxide as $ZT=0.30$ at present is evaluated as approximately one-third of the standard requirement for thermoelectric materials in practical use. However, it should be noted that the present oxide attains such ZT values by overcoming a large disadvantage due to the markedly high thermal conductivity with a predominant contribution from phonons. Because several

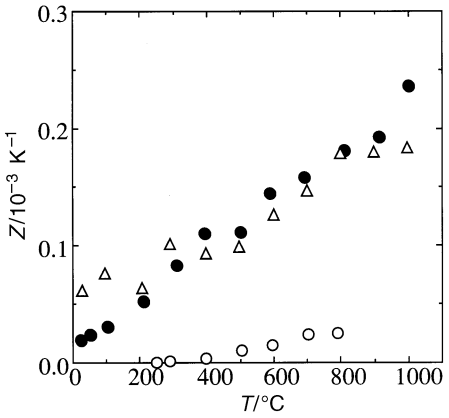

Fig. 8 The figures of merit of $(Zn_{1-x}Al_x)O$ as a function of temperature for $x=0$ (○), 0.02 (●), 0.05 (△)

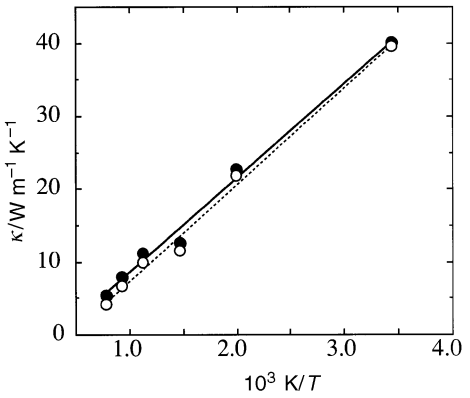

Fig. 9 The thermal conductivities of $(Zn_{0.98}Al_{0.02})O$ as a function of inverse temperature. ●, κ; ○, $\kappa_{ph}=\kappa-\kappa_e$.

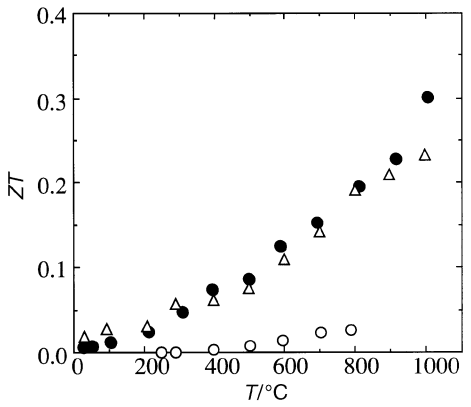

Fig. 10 The dimensionless figures of merit of $(Zn_{1-x}Al_x)O$ as a function of temperature for $x=0$ (○), 0.02 (●), 0.05 (△)

methodologies have been reported for effective reduction of the lattice thermal conductivity, circumventing degradation in the electrical properties, we can expect the ZT of $(Zn_{1-x}Al_x)O$ to improve further.

Conclusions

The thermoelectric properties of $(Zn_{1-x}Al_x)O$ were investigated and revealed to be highly promising for a potential high-temperature thermoelectric material. The σ values of $(Zn_{1-x}Al_x)O$ $(0<x\leqslant 0.05)$ were more than three orders of magnitude higher at room temperature than that of undoped ZnO, showing metallic behaviour. The absolute value of the Seebeck coefficient of $(Zn_{1-x}Al_x)O$ decreased accordingly, but remained moderate with a general trend in which $|S|$ increased gradually from *ca.* 100 μV K^{-1} at room temperature to *ca.* 200 μV K^{-1} at 1000 °C. These results appeared to be consistent with an increase in the carrier concentration by Al-doping, and were confirmed by the Hall measurements. However, we concluded that the apparent solubility limit of Al in ZnO is less than $x=0.005$ from the results of the n measurements and ^{27}Al NMR studies. The x dependence of the Hall mobility was considered to be related to the grain structures. The power factors of all the Al-doped samples attain markedly large values of $(8–15)\times 10^{-4}$ W m^{-1} K^{-2} over a range from room temperature to 1000 °C. These are the largest values of all oxides reported, and surpass those of β-$FeSi_2$ and β-SiC which have been studied extensively as high-temperature non-oxide candidates. The thermal conductivities of all the samples decreased (from *ca.* 40 W m^{-1} K^{-1} at room temperature to *ca.* 5 W m^{-1} K^{-1} at 1000 °C) with increasing temperature, and decreased with increasing amount of doped Al_2O_3. In spite of the high κ value, the oxide at $x=0.02$ attained a figure of merit of $Z=0.24\times 10^{-3}$ K^{-1} and a dimensionless figure of merit of $ZT=0.30$ at 1000 °C. The unexpectedly high thermoelectric performance of the present oxide can be attributed to the rather covalent character of the metal-to-oxygen bond in the oxide, resulting in a high carrier mobility. Although the κ values of $(Zn_{1-x}Al_x)O$ appeared to be considerably high compared to other thermoelectric materials, the lattice thermal conductivity was revealed to have the dominant contribution to the overall κ value of $(Zn_{1-x}Al_x)O$. It is therefore expected that reduction of the lattice thermal conductivity without seriously affecting the electrical properties, as has been proposed and proven to be effective in many cases, will further improve the ZT value of $(Zn_{1-x}Al_x)O$.

The authors thank Mr. Yasuhiro Yamada of the Government Industrial Research Institute, Kyushu, for his kind cooperation on the laser flash measurement of κ. We also acknowledge Professor Isao Mochida and Dr. Kinya Sakanishi of the Institute of Advanced Material Study of our University for the ^{27}Al NMR measurements.

References

1 C. M. Bhandari and D. M. Rowe, *Contemp. Phys.*, 1980, **21**, 219.
2 J. C. Bass and N. B. Elsner, in *Proc. 3rd Int. Conf. Thermoelec. Energy Conv.*, ed. K. R. Rao, IEEE, New York, 1980, p. 8.
3 J. F. Nakahara, T. Takeshita, M. J. Tschetter, B. J. Beaudry and K. A. Gschneidner Jr., *J. Appl. Phys.*, 1988, **63**, 2331.
4 I. Nishida, *Phys. Rev. B*, 1973, **7**, 2710.
5 I. Nishida and T. Sakata, *J. Phys. Chem. Solids*, 1978, **39**, 499.
6 T. Kojima, *Phys. Status Solidi A*, 1989, **111**, 233.
7 C. Wood and D. Emin, *Phys. Rev. B*, 1984, **29**, 4582.
8 S. Yugo, T. Sato and T. Kimura, *Appl. Phys. Lett.*, 1985, **46**, 842.
9 W. J. Macklin and P. T. Moseley, *Mater. Sci. Eng. B*, 1990, **7**, 111.
10 T. O. Mason, *Mater. Sci. Eng. B*, 1991, **10**, 257.
11 W. J. Macklin and P. T. Moseley, *Mater. Sci. Eng. B*, 1991, **10**, 260.
12 C. G. Fonstad and R. H. Rediker, *J. Appl. Phys.*, 1971, **42**, 2911.
13 T. P. Pearsall and C. A. Lee, *Phys. Rev. B*, 1974, **10**, 2190.
14 M. Ohtaki, D. Ogura, K. Eguchi and H. Arai, *J. Mater. Chem.*, 1994, **4**, 653.
15 M. Ohtaki, H. Koga, T. Tokunaga, K. Eguchi and H. Arai, *J. Solid State Chem.*, 1995, **120**, 105.
16 S. J. Jung, H. Ohsawa, Y. Nakamura, K. Hasumi and O. Okada, *J. Electrochem. Soc.*, 1994, **141**, L53.
17 S. N. Bai and T. Y. Tseng, *J. Appl. Phys.*, 1993, **74**, 695.
18 M. Ohtaki, T. Tsubota, K. Eguchi and H. Arai, *J. Appl. Phys.*, 1996, **79**, 1816.
19 K. Koumoto, M. Shimohigasi, S. Takeda and H. Yanagida, *J. Mater. Sci. Lett.*, 1987, **6**, 1453.
20 G. Heiland, E. Mollwo and F. Stuöckmann, *Solid State Phys.*, 1959, **8**, 191.
21 M. Nakamura, N. Kimizuka, T. Mohri and M. Isobe, *J. Solid State Chem.*, 1993, **105**, 535.
22 J. W. Akitt, in *Multinuclear NMR*, ed. J. Mason, Plenum Press, New York, 1987, p. 259.
23 B. C. Gerstein, *Anal. Chem.*, 1983, **55**, 781A.
24 A. F. Ioffe, *Semiconductor Thermoelements and Thermoelectric Cooling*, Infosearch Limited, London, 1957.
25 R. P. Chasmer and R. J. Stratton, *J. Electron. Control*, 1959, **7**, 52.
26 T. Caillat, A. Borshchevsky and J-P. Fleurial, in *Proc. 13th Int. Conf. Thermoelectrics*, 1994, ed. B. Mathiprakasem, ALP Press, New York, p. 58.
27 T. Caillat, A. Borshchevsky and J-P. Fleurial, in *Proc. 13th Int. Conf. Thermoelectrics*, ed. B. Mathiprakasem, ALP Press, New York, 1994, p. 31.
28 T. Caillat, A. Borshchevsky and J-P. Fleurial, in *Proc. 13th Int. Conf. Thermoelectrics*, 1994, ed. B. Mathiprakasem, ALP Press, New York, p. 209.
29 J. C. Phillips, *Rev. Mod. Phys.*, 1970, **42**, 317.
30 C. Kittel, *Introduction to Solid State Physics*, 6th edn., Wiley, New York, 1986.
31 M. E. Fine and N. Hsieh, *J. Am. Ceram. Soc.*, 1974, **57**, 502.

Paper 6/02506D; *Received* 10*th April*, 1996